mathematics

MDPI

Article

Thermal Conductivity and Thermophoretic Impacts of Micropolar Fluid Flow by a Horizontal Absorbent Isothermal Porous Wall with Heat Source/Sink

Hossam A. Nabwey [1,2,*], Ahmed M. Rashad [3], Abd El Nasser Mahdy [4] and Shaaban M. Shaaban [2,5]

[1] Department of Mathematics, College of Science and Humanities in Al-Kharj, Prince Sattam bin Abdulaziz University, Al-Kharj 11942, Saudi Arabia
[2] Department of Basic Engineering Science, Faculty of Engineering, Menoufia University, Shebin El-Kom 32511, Egypt; shabaan27@gmail.com or shaban.awdallah@nbu.edu.sa
[3] Mathematics Department, Faculty of Science, Aswan University, Aswan 81528, Egypt; am_rashad@yahoo.com or am_rashad@aswu.edu.eg
[4] Department of Mathematics, Faculty of Science, South Valley University, Qena 83523, Egypt; mahdy@svu.edu.eg
[5] Department of Electrical Engineering, College of Engineering, Northern Border University, Arar 1321, Saudi Arabia
* Correspondence: h.mohamed@psau.edu.sa or eng_hossam21@yahoo.com

Abstract: Boundary layer analysis is invoked to clarify the aspects of variable thermal conductivity and thermophoretic forces on a steady state of MHD micropolar fluid flow in the existence of a uniform transverse magnetic field along an isothermal horizontal plate. The micropolar pattern permits the rotational freedom degrees that lead to couple stresses and a non symmetric stress tensor. The initiated PDEs governing the case pattern are mutated into a non-dimensional system due to proper transformations. The transformed mathematical governing equations are solved by implementing a very potent computer algebra software MATLAB code. The plotted graphs analyzed the attitude of multiple physical aspects involving factors on the flow attitude of micropolar velocity and angular velocity and temperature. Through the involved factors, the couple stress, skin friction and Nusselt number are manifested and interpreted amply. A new outcome for drag force and heat gradient experienced by the key factors is portrayed. Augmentation in Ω results in the thermophoretic forces that encapsulate the mass transmission. The local Nusselt number strengthened as the thermal conductivity, heat absorption factors or wall suction velocity were improved, and weakened due to the existence of viscous dissipation or heat generation impacts. As a particular case, the governing field equations of a classical Newtonian liquid are given by dropping the micropolar parameter impacts.

Keywords: micropolar; porosity; thermal conductivity; viscous heating; thermophoretic

MSC: 76-10; 76A05; 76D05; 76W05

Citation: Nabwey H.A.; Rashad, A.M.; Mahdy, A.E.N.; Shaaban, S.M. Thermal Conductivity and Thermophoretic Impacts of Micropolar Fluid Flow by a Horizontal Absorbent Isothermal Porous Wall with Heat Source/Sink. *Mathematics* **2022**, *10*, 1514. https://doi.org/10.3390/math10091514

Academic Editor: James M. Buick

Received: 31 March 2022
Accepted: 29 April 2022
Published: 2 May 2022

1. Introduction

A number of industrially significant fluids exhibit a non-Newtonian fluid attitude. Due to the growing usage of these non-Newtonian liquids, massive efforts have been directed toward realizing their flow and heat transfer behaviors. The non-Newtonian liquids, which can be seen in heterogeneous mixtures, colloidal liquids, animal blood, exotic lubricants, most slurry and a number of liquids with polymer additives, have microstructure, which is randomly oriented or composed of spherical elements in a viscous medium, and hence they do not undergo the Newtonian liquid flow theorem. For illustrating and understanding the attitude of such liquids, there were several non-Newtonian liquid theorems invoked. Convenient contributions [1–9] have been presented on non-Newtonian liquid motion

over variant geometrical surfaces. Among these, the micropolar liquid theorem stated by Eringen [10,11] has special features, such as microscopic impacts due to the local structure and micromotion of liquid elements, and not the absence of couple stresses, body couples and non-symmetric stress tensors. Therefore, it may be applied to explore the attitude of blood flow, colloidal suspensions or polymeric additives, liquid crystals and dirty oils, and exotic lubricants. The distinct features of micropolar liquids were argued in a comprehensive review article of the application of micropolar liquid mechanics by Ariman et al. [12]. Nabwey and Mahdy [13] reported the attitude of momentum and heat transmission of homogeneous dust elements micropolar fluid flow along a vertical permeable cone with variable wall temperature and suction impacts. MHD flow and heat transmission attitude of a viscous electrically conducting incompressible micropolar liquid through a channel due to a shrinking and a stationary surface and rotating disks has been examined by Ali et al. [14,15].

The phenomenon of the movement of loaded molecules in a liquid that leads to thermal gradient and the flow of elements continually reversing to the thermal gradient is known as thermophoresis. The forces of thermophoresis are very important in natural convection by the lower liquid velocities. Additionally, the velocity of thermophoresis is permanently boosted by the loaded liquid elements in the direction of declining thermal gradient. Hazarika and Ahmed [16,17] have recognized the impact of thermophoresis in their new investigations on heat and mass transfer and introduced detailed clarifications. In addition, due to physical technique, viscous dissipation represents the produced kinetic energy altered into thermal energy, which may be noticed in natural convection concerned with dawdled speed from high rotating speeds. Buoyancy forces arising from thermal and mass diffusion are of wide importance in miscellaneous industrial operations, e.g., geo-physics, solidification of binary alloys and chemical engineering. Commonly, this outcome is indicated by the Eckert number, and a lot of researchers have exhibited its impact. Tsai [18], Talbot et al. [19] and Chamkha and Camille [20] have illustrated that the result of thermophoretic forces on the exchange of heat and mass flow is ostentatiously clarified. The authors scrutinized the significance of heat absorption/generation and explored the aspect of suction and thermodiffusion in 2-D laminar flow over flat plates for boosted values of physical factors.

Based on the miscellaneous applications of magnetohydrodynamics (MHD), there has been a focus on realizing fluid movement attitude in which the liquid attitude of electrically conducting and magnetic features has been examined. MHD applications can be noticed in liquid metals, power generation, plasma, etc. Miscellaneous analyses have been provided with several aspects of MHD flows of different types of fluids [21–25]. The impact of viscous dissipation and chemical reaction on mass and heat transmit flow of magnetohydrodynamic of micropolar liquid has been argued by Sheri and Shamshuddin [26]. Shehzad et al. [27] handled numerically the problem of MHD flow of non-Newtonian nanofluid due to convective boundary conditions. In addition, fluid motion within porous media has become very significant because of ground water flows and miscellaneous tertiary oil retrieval operations. Again, there are a variety of practical applications of liquid movement within porous media, involving filtration flow in packed columns, permeation of water or oil within matrix of porous rock, etc. The Darcy equation is known to be strong in describing this flow. Several researchers [28–33] have concentrated fluid flows within a porous media in miscellaneous flow cases.

As the surface is cooling or heating, the viscous dissipation values and Joule heating become more significant. Massive engineering and industrial operations of Joule heating phenomena may be noticed such as sterilization, electronic chips, electric coffee fabricators, cooling of metallic sheets, cooling of nuclear reactors, system of power generators and food processing. The heat energy is established in the Joule heating due to an electric current on the conductor. The major utility of Joule heating is transmitting an electrical intensity to lessen the damages by reducing the current. The magnetohydrodynamics of non-Newtonian micropolar liquid flow with heat absorption/generation through an

extending plate has been reported by Khedr et al. [34]. Hayat et al. [35] provided the viscous dissipation impact in Burger's fluid flow. Joule heating in MHD nanoliquid flow with slip condition was performed by Alreshidi et al. [36]. Hayat and Qasim [37] presented Joule heating in MHD non-Newtonian Maxwell fluid flow. Shah et al. [38] exhibited viscous dissipation and Joule heating impacts in Ag-H_2O nanofluids. The impact of heat source/sink in the magnethydrodynamics of non-Newtonian fluid flow has been analyzed by Sandeep and Sulochana [39]. Further related contributions can be seen in Refs. [40–43].

Due to the invoked literature review, our analysis initiates the impact of variable thermal conductivity and thermophoretic forces and porosity of Darcy regime on 2-D MHD micropolar fluid flow around an isothermal horizontal porous wall inspired by the applications of Joule heating. The governing non-linear PDEs are turned into ODEs utilizing similarity transformation, and a tool using finite difference technique of bvp4c code has been initiated to gain the numerical computations of the non-linear ODEs concerned with convenient boundary conditions. The significant computations have portrayed through curves with the help of MATLAB codes. It is possible that the current contribution may be considered as a vehicle to understand the particle deposition phenomenon with the existence of magnetic field and a heat source of a sink. blowing. The significance of porous media and such contribution can be seen in variant branches such as petroleum engineering, biophysics, hydrogeology, material science, etc.

2. Flow Equations Analysis

Figure 1 illustrates a 2-D steady flow of non-Newtonian (of micropolar type) electronically conducting fluid through a horizontal isothermal plate placed in a Darcy porous domain due to heat generation and variable thermal conductivity. The surface temperature is T_w, and the concentration at the surface is selected to be zero $C_w = 0$. The temperature and concentration far away from the boundary layer are T_∞, C_∞. A coordinate system (x, y) is presented as shown. Moreover, a non-variable magnetic field $(0, H_0, 0)$ is imposed as normal to the x-axis. Due to the surface wall of tiny pores, the velocities of suction and injection are applicable with an angle $\pi/2$ to the wall. The non-Newtonian micropolar fluid molecules move along the wall. Via the help of forgoing assumptions and Boussinesq approximations, the governing flow equations for the considered pattern are stated as [8,18,20].

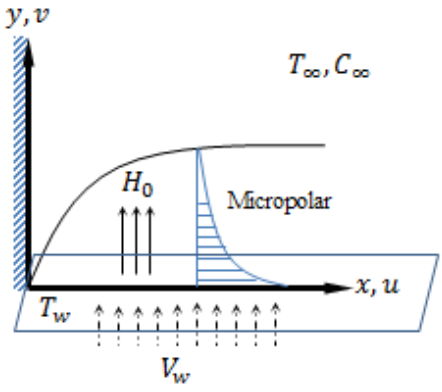

Figure 1. Geometrical coordinates and physical model.

$$\frac{\partial u}{\partial x} + \frac{\partial v}{\partial y} = 0 \tag{1}$$

$$u\frac{\partial u}{\partial x} + v\frac{\partial u}{\partial y} = \left(\nu + \frac{\varrho}{\rho}\right)\frac{\partial^2 u}{\partial y^2} - \left(\frac{\sigma H_0^2}{\rho} + \frac{\nu}{\tilde{K}}\right)(u - \mathrm{U}) + \frac{\varrho}{\rho}\frac{\partial \tilde{N}}{\partial y} \tag{2}$$

$$u\frac{\partial \tilde{N}}{\partial x} + v\frac{\partial \tilde{N}}{\partial y} = \frac{\tilde{\xi}}{j\rho}\frac{\partial^2 \tilde{N}}{\partial y^2} - \frac{\varrho}{j\rho}\left(2\tilde{N} + \frac{\partial u}{\partial y}\right) \tag{3}$$

$$\rho c_p\left(u\frac{\partial T}{\partial x}+v\frac{\partial T}{\partial y}\right)=\frac{\partial}{\partial y}\left(k\frac{\partial T}{\partial y}\right)+(\mu+\varrho)\left(\frac{\partial u}{\partial y}\right)^2+\sigma H_0^2(u-\mathrm{U})^2+\tilde{Q}(T-T_\infty) \quad (4)$$

$$u\frac{\partial C}{\partial x}+v\frac{\partial C}{\partial y}=D\frac{\partial^2 C}{\partial y^2}-\frac{\partial}{\partial y}(\bar{V}C) \quad (5)$$

where the convenient boundary conditions considered here are [8,18,20].

$$\begin{aligned} &u=0, \quad v=-V_w, \quad \tilde{N}=-m\frac{\partial u}{\partial y}, \quad T=T_w, \quad C=0 \qquad \text{at} \quad y=0\\ &u\to \mathrm{U}, \quad \tilde{N}\to\tilde{N}_\infty, \quad T\to T_\infty, \quad C\to C_\infty, \qquad \text{as} \quad y\to\infty \end{aligned} \quad (6)$$

In earlier governing flow equations, u and v present the non-Newtonian micropolar velocity components through the trends of x and y axes, respectively; ρ indicates the active density of the fluid; μ stands for the effective dynamic viscosity of micropolar fluid; ϱ is the vortex viscosity; $\tilde{K}$ is the porosity factor; T, C point out the temperature and concentration; and g represents the acceleration due to gravity. Additionally, $\tilde{\xi}$ symbolizes the viscosity of the spin gradient, and there is considered to be a linear relation between the spin gradient viscosity $\tilde{\xi}$ and the microinertial coefficient j in the formula $\tilde{\xi}=(\mu+0.5\varrho)j$ like [5,8]. The microrotation factor m appearing in boundary conditions has the range $0\le m\le 1$. A zero value of m, i.e., $m=0$, refers to intense concentration of microelements, whereas $m=1/2$ indicates low microelements concentration, $\tilde{Q}$ gives the dimensional heat generation factor, m gives microrotation factor, and $\tilde{N}$ is the angular velocity. The thermophoretic velocity $\bar{V}$ appears in Equation (5) is assigned as in [18–20].

$$\begin{aligned} \bar{V}&=-\lambda\nu\frac{\nabla T}{T}=-\frac{\lambda\nu}{T}\frac{\partial T}{\partial y}=\frac{\Omega\nu}{T_w-T_\infty}\frac{\partial T}{\partial y},\\ \lambda&=\frac{2C_s(k/k_p+C_tK_n)C_n}{(1+3C-mK_n)(1+2k/k_p+2C_tK_n)} \end{aligned} \quad (7)$$

The factor of λ is commonly considered to vary from 0.2 up to 1.2 [18]. Let us assign the thermophoretic factor $\Omega=-\lambda(T_w-T_\infty)/T$, with $\Omega=0.01, 0.1$, and 1.0, whose associated values of $-\lambda(T_w-T_\infty)$ were approximately 3, 30 and 300 K for a temperature 300 K. Again, the variable thermal conductivity k is expressed as

$$k=k_f(1+\delta(T-T_\infty))=k_f(1+\gamma\theta) \quad (8)$$

where T_∞ presents the temperature of the free stream; k, k_f point out the thermal conductivities at temperatures T and T_∞, respectively; δ stands for the fluid trustworthy thermo-physical fixed value, with negative values of δ assigning lubricant liquids and positive values of δ providing air or water; and the factor γ equals $\delta(T-T_\infty)$.

At this stage, let us assign the next non-dimensional functions ψ, θ, ϕ and η as follows:

$$\begin{aligned} &\eta=\left(\frac{\mathrm{U}}{2\nu x}\right)^{1/2}y, \quad \psi=(2\nu x\mathrm{U})^{1/2}F(\eta), \quad N(\eta)=\left(\frac{2\nu x}{\mathrm{U}^3}\right)^{1/2}\tilde{N}\\ &\theta(\eta)=\frac{T-T_\infty}{T_w-T_\infty}, \qquad \phi(\eta)=\frac{C}{C_\infty} \end{aligned} \quad (9)$$

ψ points out stream function, and in terms of previous mathematical expressions (u, v) components can be stated as

$$u=\frac{\partial\psi}{\partial y}=\mathrm{U}F'(\eta), \quad v=-\frac{\partial\psi}{\partial x}=-\frac{1}{2}\left(\frac{2\nu\mathrm{U}}{x}\right)^{1/2}F(\eta) \quad (10)$$

Utilizing Equation (9), therefore, the flow governing equations Equations (2)–(5) are reduced to

$$(1+\beta)F''' + FF'' - (H_a^2 + K^{-1})(F'-1) + \beta N' = 0 \tag{11}$$

$$\left(1+\frac{1}{2}\beta\right)N'' + FN' + F'N - \beta\omega(2N+F'') = 0 \tag{12}$$

$$Pr^{-1}\left((1+\gamma\theta)\theta'' + \gamma\theta'^2\right) + F\theta' + Ec(1+\beta)F''^2 + EcH_a^2\,(F'-1)^2 + Q\theta = 0 \tag{13}$$

$$Sc^{-1}\phi'' + (F - \Omega\theta')\phi' - \Omega\phi\theta'' = 0 \tag{14}$$

and the given boundary conditions mutated into

$$\begin{aligned} &F(0) = f_w, \quad F'(0) = 0, \quad N(0) = -mF''(0), \quad \theta(0) - 1 = \phi(0) = 0, \\ &F'(\infty) \to 1, \quad N(\infty) \to 0 \quad \theta(\infty) \to 0, \quad \phi(\infty) \to 1 \end{aligned} \tag{15}$$

wherein primes "′" refer to differentiation with respect to similarity variable η; $\beta = \rho/\mu$ and $\omega = 2\nu x/(\mathrm{U}j)$ symbolize the micropolar material factors; $H_a^2 = 2\sigma H_0^2 x/(\mathrm{U}\rho)$ indicates magnetic field factor; $Q = 2x\tilde{Q}/(\mathrm{U}\rho c_p)$ points out the heat source or sink factor; $Ec = \mathrm{U}^2/(c_p(T_w - T_\infty))$ is the Eckert number; $Pr = \mu c_p/k_f$ stands for the Prandtl number; $Sc = \nu/D$ is the Schmidt number; $K = \tilde{K}\mathrm{U}/(2\nu x)$ is the porosity factor; and $f_w = 2V_w(x/2\nu\mathrm{U})^{1/2}$ is the suction/blowing flow factor.

Finally, in order to view the attitude of the pattern of current non-Newtonian micropolar fluid flow, the quantities of physical significance are expressed as the local skin friction factor C_f, the couple stress factor Nn_x, the local heat transmission factor Nu_x and mass transmission factor Sh_x, and those are formulated as

$$\begin{aligned} C_f &= \frac{\tau_w}{\rho\mathrm{U}^2}, & Nn_x &= \frac{2xJ_w}{\rho\mathrm{U}^2 j} \\ Nu_x &= \frac{xq_w}{k_f(T_w - T_\infty)}, & Sh_x &= \frac{xq_m}{DC_\infty} \end{aligned} \tag{16}$$

where τ_w, J_w, q_w and q_m are determined by

$$\begin{aligned} \tau_w &= \left((\mu+\varrho)\frac{\partial u}{\partial y} + \varrho\tilde{N}\right)_{y=0}, & J_w &= \tilde{\xi}\left(\frac{\partial \tilde{N}}{\partial y}\right)_{y=0} \\ q_w &= k_f\left(\frac{\partial T}{\partial y}\right)_{y=0}, & q_m &= -D\left(\frac{\partial C}{\partial y}\right)_{y=0} \end{aligned} \tag{17}$$

Invoking the presented non-dimensional transformations (10), one obtains

$$\begin{aligned} &C_f Re_x^{1/2} = (1+\beta)F''(0) + \beta N(0), \quad Nn_x = (1+0.5\beta)N'(0) \\ &2Nu_x = -Re_x^{1/2}\theta'(0), \qquad 2Sh_x = -Re_x^{1/2}\phi'(0) \end{aligned} \tag{18}$$

Re_x, which equals $2x\mathrm{U}/\nu$, is known as the Reynolds number.

3. Results and Discussion

Governing flow Equations (10) through (13) relate to the boundary condition; Equation (14) illustrates the mutated similarity equations of the controlling momentum, energy and concentration equations, respectively. These non-linear differential equations have been tackled numerically by means of an efficient, iterative and finite-difference with MATLAB code. The MATLAB built-in function bvp4c [44] integrates a system of differential equations of the form $y' = f(x,y)$, subject to the boundary conditions with nonlinear shooting technique. In the shooting scheme, first-order ODEs along with initial conditions are integrated with the utilization of RK4 approach and modified missing initial conditions with the utilization of Newton's scheme until the solution meets the specified

accuracy. The asymptotic convergence is noted to be achieved for $\eta = 5$. The function bvp4c represents one of the boundary value problem solvers in the MATLAB package. MATLAB software has been used where we performed a finite difference scheme, which is a collocation method of order four. All the numerical results achieved in this problem are subjected to an error tolerance of 10^{-6}. The system of partial differential equations (PDEs) is mutated into first-order ordinary differential equations. A representative collection of numerical outcomes is given graphically in following figures to exhibit the impact of the miscellaneous physical factors on the solution. In our investigation, the given results are computed for wide ranges of the controlling factors, that is $0 \leq \beta \leq 3$, $0 \leq \gamma \leq 1$, $0.01 \leq \omega \leq 1$, $-1 \leq Q \leq 1$, $0.5 \leq Ec \leq 1.5$, $0.2 \leq K \leq 5$, $1 \leq H_a^2 \leq 10$, $0 \leq m \leq 1$ and $-1 \leq f_w \leq 1$, and we have chosen the default factors as $f_w = 0.5$, $\mathrm{Pr} = 0.71$, $\beta = \gamma = 0.4$, $Sc = 0.62$, $\omega = 1$, $\Omega = 0.1$, $m = 0.5$, $Ha = 2$, $Ec = K = 0.2$ and $Q = 0.6$, otherwise reminded. For authenticating the soundness of our numerical approach, Table 1 gives comparison data of $-\phi'(0)$ determined in our investigation and those calculated earlier by Chamkha and Camille [20] and Tsai [18]. It can be clearly seen that an excellent agreement between the data exists. This lends effectiveness to our numerical approach.

Table 1. Values of $-\phi'(0)$ for values of Ω and f_w with dropping micropolar factors.

f_w	Ω	Chamkha and Camille [20]	Tsai [18]	Present
0.5	0.02	−0.967014	−0.967530	−0.966182
	0.20	−0.983710	−0.984805	−0.984291
	2.00	−1.152172	−1.152437	−1.152257
−0.5	0.02	−0.354171	−0.354261	−0.352051
	0.20	−0.367250	−0.367710	−0.367207
	2.00	−0.548181	−0.548312	−0.547344

Figure 2 introduces the impact of coupling factor β (=0, 0.5, 1, 2 and 3) on dimensionless velocity and microrotation velocity or angular velocity. The coupling of linear and rotational movement inducing from the micromotion of the fluid elements is described by coupling factor. Therefore, the factor β signifies the coupling between the rotational and Newtonian viscosities. When $\rho - 0$, that is, $\beta = 0$, micropolarity will be lost and hence the liquid behaves as a non-polar liquid. Thus, $\beta = 0$ corresponds to viscous liquid. The figure illustrates that the velocity weakens as β boosts. The figure also portrays that the microrotation component reduces with an increment in the value of the coupling factor, and an increment in temperature variations due to the β factor.

Figure 3 demonstrates the impact of the wall mass transfer factor fw on the micropolar velocity, microrotation and temperature curves, respectively. The application of wall fluid suction, i.e., f_w, has positive values since this case has the aspect of decreasing all of the hydrodynamic and angular velocity boundary layers, causing the working fluid velocity and its microrotation to strengthen, as observed as the microrotation curves argued close to the wall then reduced far away from the plate. Moreover, the imposition of wall liquid injection $f_w < 0$ leads to an inverse impact, namely a reduction in the liquid velocity and concentration and an enhancement in its temperature. These impacts are accompanied by maximizing in all of the hydrodynamic, thermal boundary layers.

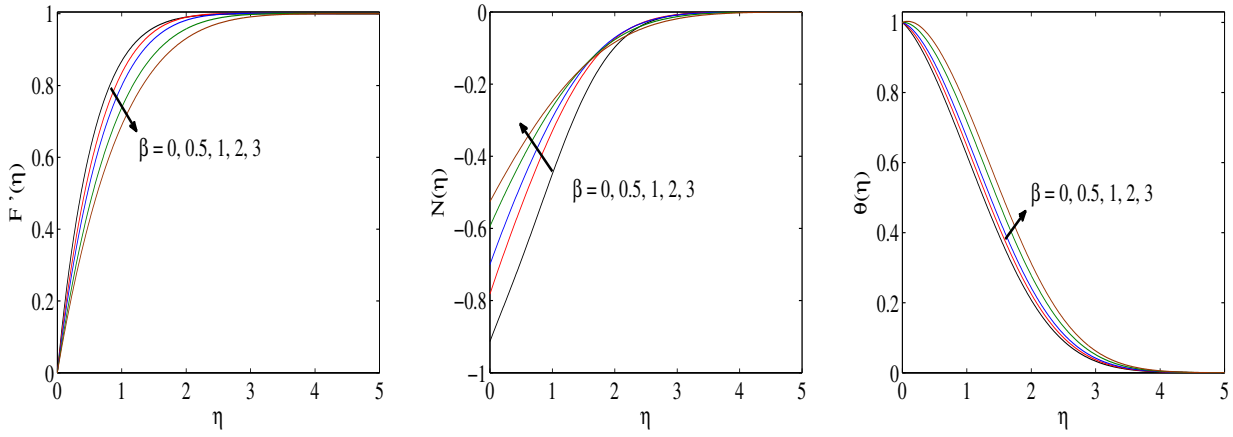

Figure 2. Velocity and angular velocity distribution under the impact of β factor.

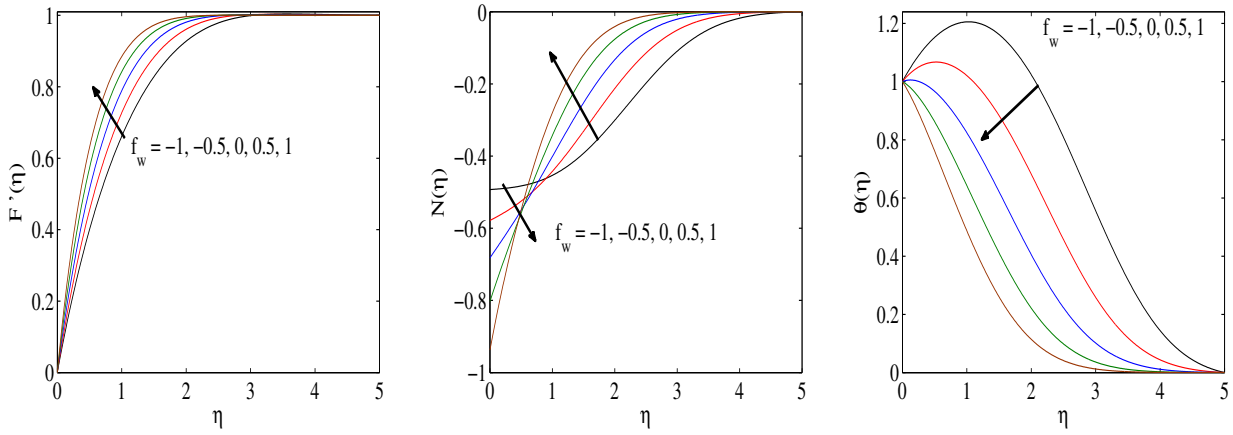

Figure 3. Velocity and angular velocity distribution under the impact of f_w factor.

Typical fluctuations for the working fluid velocity, microrotation and temperature for miscellaneous values of the Hartmann number H_a, respectively, for a physical view with heat generation and thermophoretic impacts, are depicted in Figure 4. According to the conventional Hartmann movement, the H_a affects the U due to the term $(u - \mathrm{U})$ in Equations (2) and (3), which makes the fluid velocity faster. Imposition of a magnetic field moving with the free stream has the susceptibility to result in a motive force (Lorentz force) which accelerates the fluid flow and its angular velocity and weakens its boundary layer. This is accompanied by accelerating the working liquid temperature. Moreover, the thermal boundary layer becomes thicker as a result of escalating the strength of applied H_0.

The attitude of porosity factor K over the working liquid velocity F', angular velocity N and temperature θ under the action of suction ($f_w = 0.5$) are sketched in Figure 5. The imposition of porosity K into the boundary layer indicates that the fluid elements are restricted to flow from the wall to the fluid zone, which yields the velocity to be slow and and angular. Physically, as the quantity of Joule heating $EcH_a^2(F' - 1)^2$ increases from F' to $(F' - 1)$, it results in higher temperature profiles. Within thermal boundary layer, the fluid elements are flowing past the monotonically enhancing fluctuations of θ due to the impact of K. In addition, letting $m = 0$ results in zero microrotation (no-spin condition), and due to the condition at the porous wall $N(0) = -mF''(0)$, the microelements in the flow of concentrated particles close to the wall cannot spin. When $m = 0.5$ (N cannot vanish when $F''(0) \neq 0$), the part that is anti-symmetric from the stress tensor vanishes and gives a weak concentration. The element spin for fine molecules loaded is to be equal to the velocity of the working fluid at the porous wall. As $m = 0.5$, it has the potential to illustrate the possibility of diminishing the ruling equations to the equations of Newtonian case ($\rho = 0$).

For the purpose of modeling the turbulent boundary layer flows, we have $m = 1$. As is clear, the velocity becomes faster with an increment of m factor, but an opposite attitude for angular velocity and temperature profiles is shown in Figure 6.

Figure 7 clarifies the variation in thermal distribution versus Eckert number Ec in the case of positive and negative values of f_w. Actually, the Eckert number represents the ratio of advective transport to the heat dissipation potential. The supporting miscellaneous values suggest cooling of the surface, that is, a diminution of high temperature from the wall to the working liquid, such that the higher Joule heat values provide the variation in temperature fluctuations. Again, the variation in thermal fluctuation is higher in cases of injection flow as compared to suction flow cases. The second part of Figure 7 indicates the impact of the non-dimensional heat generation or absorption factor Q on the working fluid temperature variations. As stated before, owing to the existence of a heat source or heat generation impact (i.e., Q is positive), the temperature fluctuations of the working liquid strengthen, causing the thermal boundary layer to be thicker. In the situation that the magnitude of the heat source is comparatively large, the highest working fluid temperature is not noticed at the wall but rather in the liquid domain close to it. Contrariwise, the existence of a heat sink or a heat absorption impact (i.e., Q is negative) causes the thermal state of the liquid to weaken, thus outputting a thinner thermal boundary layer. The last part of Figure 7 points out the impact of γ factor for $f_w = 0.5$ and -0.5. The factor γ represents thermal conductivity or the capability of a material to deport heat, and the value of heat is transported by conduction through a unit area of a cross-section of a material; as a temperature gradient gets out perpendicular to the area, this provides Fourier's law of heat conduction. Due to the heat conduction law, heat flux is directly proportional to $\partial T/\partial y$, and the proportionality constant γ is known as the thermal conductivity, which relates to the variant in temperature in the heat flux trend.

In effect, thermal conductivity and porosity have wide significance in the manufacturing of nano-materials in mechanical engineering applications. It is illustrated that temperature distributions rise (in the last part of Figure 7) with an increment in the γ factor. In the case of injection, the temperature distribution decreases until the value of η equals 1.528, and then it upgrades. Figure 8 signposts the impact of thermophoretic forces Ω on the distributions of ϕ. The phenomenon of thermophoresis may be noticed in the collection of movable elements, in which the force of a temperature gradient can be seen due to the different responses given by several types of elements. From a physical point of view, thermophoretic forces Ω result in a gradient of temperature between the heated working liquid and the cold surface that affects the flow of the molecules of micropolar fluid close to the porous wall. In any case, due to the cause of the thermophoretic forces, the working fluid velocity is weakened, whereas ϕ distributions are boosted. In addition, the factor Ω represents a decreasing function of mass transfer, since augmentation in Ω results in the thermophoretic forces that encapsulate the mass transmission. The variations in skin friction C_f, couple stress Nn_x coefficients and Nusselt number Nu_x against coupling factor β are presented in Figure 9. As is clear from the figure, enlarging values of coupling factor β lead to an augmentation of skin friction and couple stress coefficients as well as a reduction in the Nusselt number. Figure 10 depicts the deviation of Eckert number Ec, heat generation/absorption Q and variable thermal conductivity factor γ over the heat transmission expressed in Nusselt number Nu_x at the wall $\eta = 0$ for $f_w = 0.5$. The Nusselt number is a monotonic reducing function of the Eckert number and heat sink parameter, whereas it represents an increasing function of thermophoretic and heat source factors.

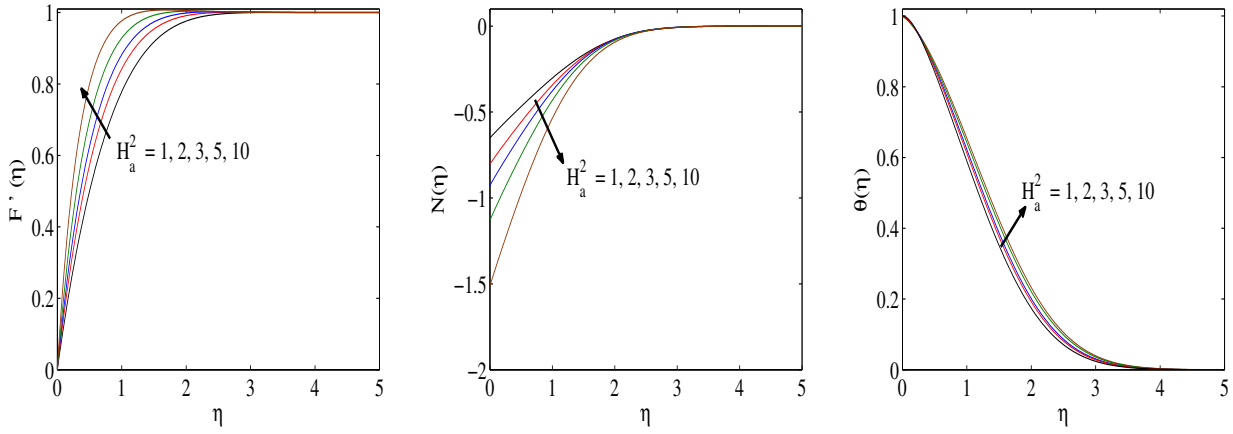

Figure 4. Velocity and angular velocity distribution under the impact of *Ha* factor.

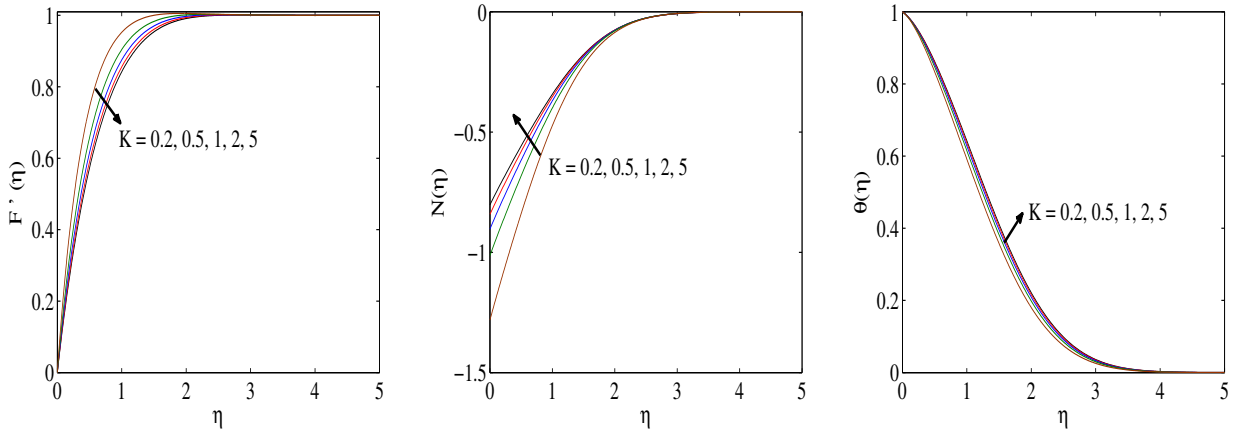

Figure 5. Velocity and angular velocity distribution under the impact of *K* factor.

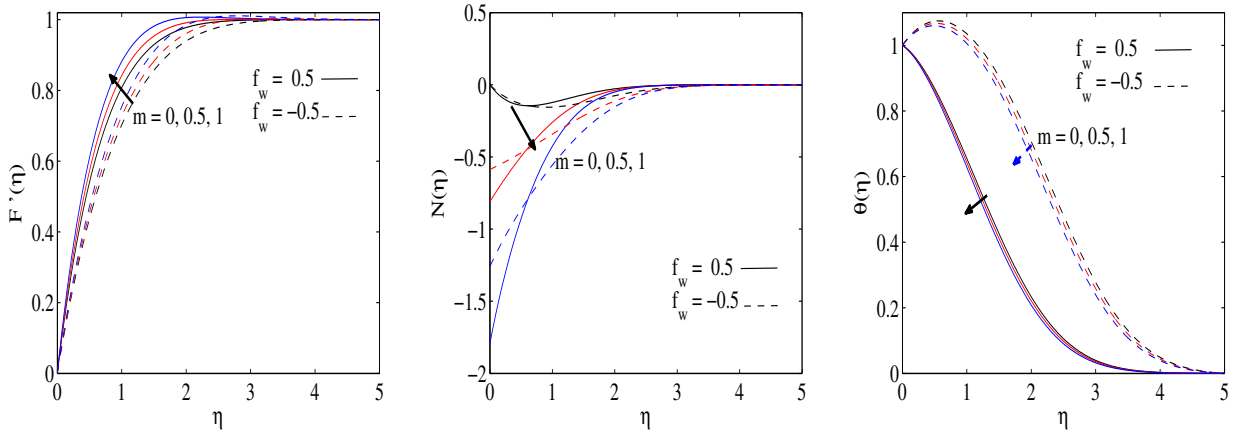

Figure 6. Velocity and angular velocity distribution under the impact of *m* factor.

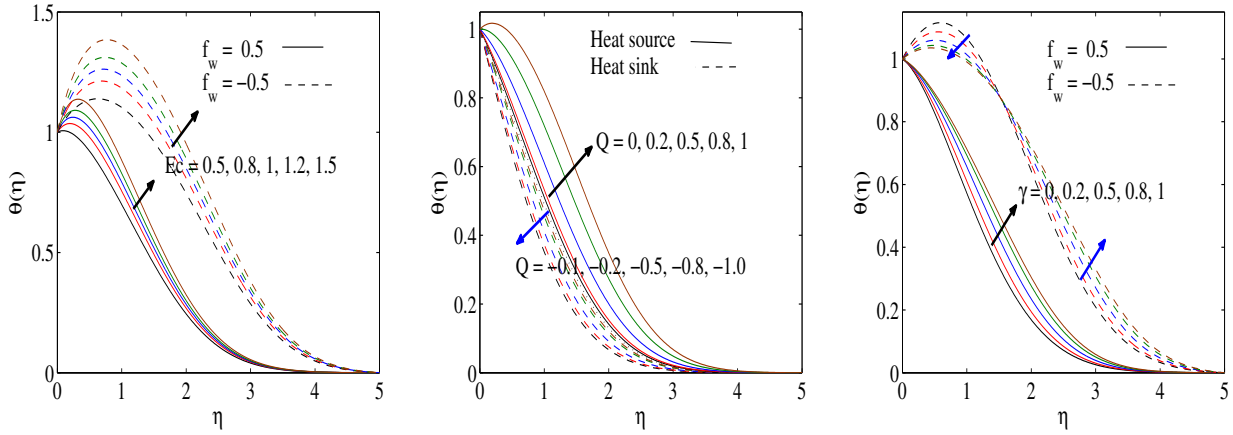

Figure 7. θ fluctuations under the impact of Ec, Q and γ factors.

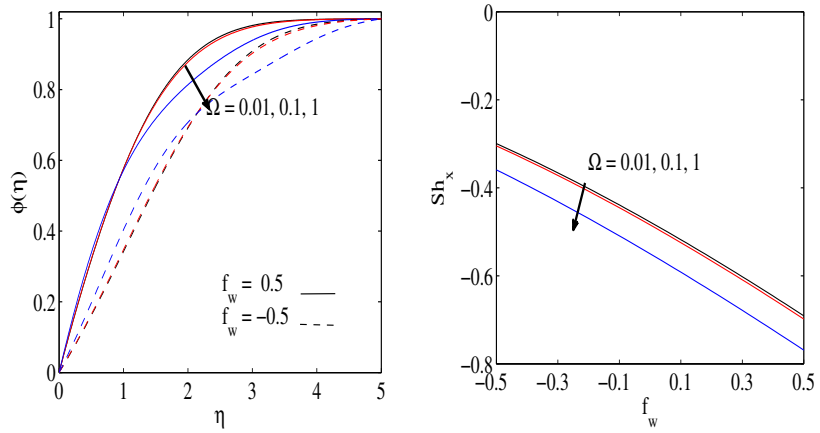

Figure 8. ϕ and sh_x fluctuations under Ω factor impact.

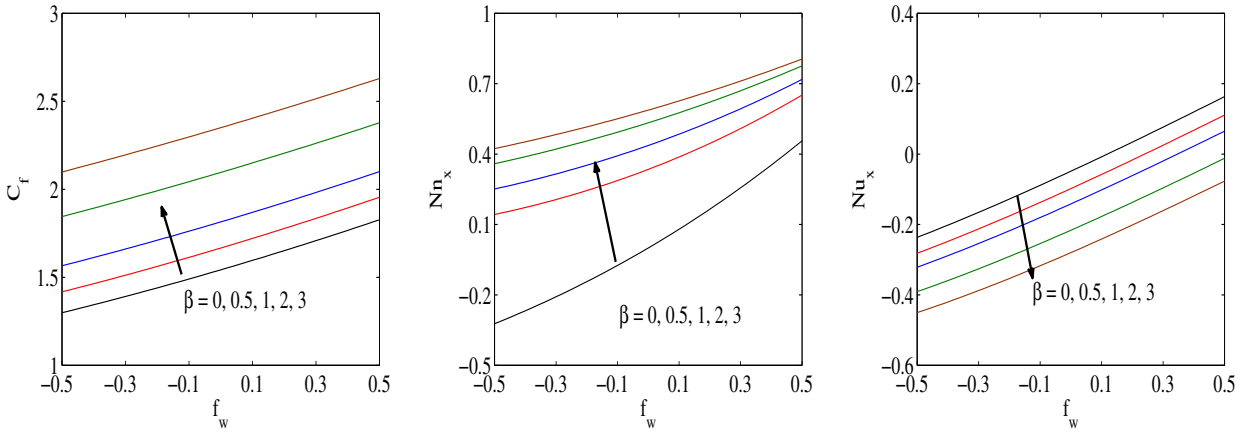

Figure 9. C_f, Nn_x and Nu_x under the impact of β factor.

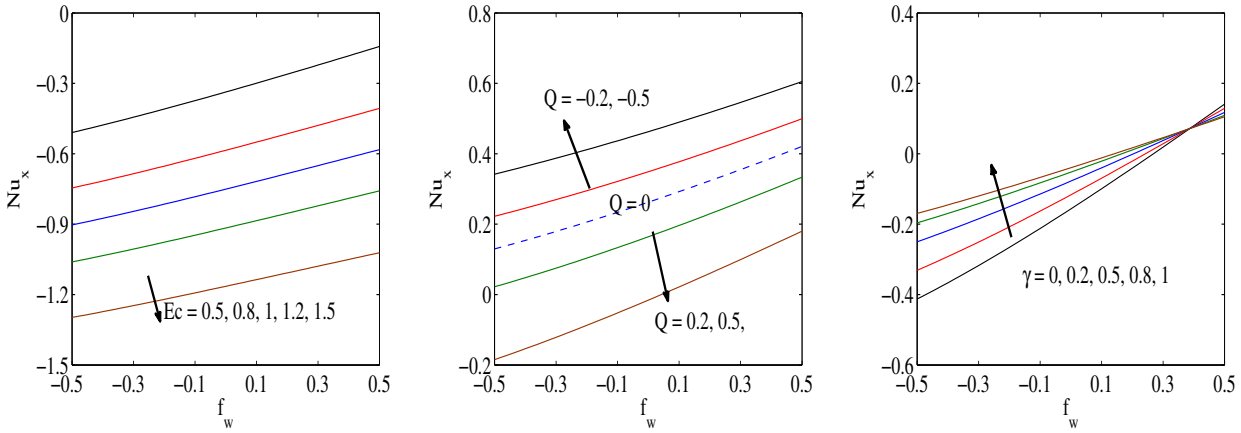

Figure 10. Nu_x under the impact of Ec, Q and γ factors.

4. Conclusions

The impact of wall suction or injection, variable thermal conductivity and thermophoresis on laminar MHD non-Newtonian micropolar fluid flow over an isothermal porous wall has been studied. A set of similarity equations controlling the fluid velocity, microrotation, temperature and element mass concentrations has been provided by employing a similarity transformation. It is possible that the current contribution may be considered as a vehicle to understand the particle deposition phenomenon with the existence of the magnetic field and heat source of a sink. From the introduced contributions, the following conclusion items are drawn:

- An augmentation in Ω results in the thermophoretic forces that encapsulate the mass transmission.
- An enhancement in the magnetic field factor has the same impact on the flow distribution as an increment in viscosity.
- The local Nusselt number strengthened as the thermal conductivity, heat absorption factors or wall suction velocity were boosted, and weakened due to the existence of either heat generation or viscous dissipation impacts.
- The temperature profiles boost with enlarging Eckert numbers, porosity and magnetic factors.
- The coupling factor leads to amplifying skin friction and couple stress while lessening the Nusselt number.
- Heat source results in a thicker boundary layer, while heat sink leads to a thinner thermal boundary layer.
- The microrotation fluctuations are enhanced in the case of strong ($m = 0$) and low ($m = 0.5$) concentrations and are weakened in the case of a very low ($m = 1$) concentration.

Author Contributions: Formal analysis, H.A.N., A.M.R., A.E.N.M. and S.M.S.; Methodology, H.A.N., A.M.R., A.E.N.M. and S.M.S.; Project administration, H.A.N.; Writing—original draft, H.A.N., A.M.R., A.E.N.M. and S.M.S.; Writing—review and editing, A.M.R., A.E.N.M. and S.M.S. All authors have read and agreed to the published version of the manuscript.

Funding: The authors extend their appreciation to the Deputyship for Research and Innovation, Ministry of Education in Saudi Arabia, for funding this research work through the project number (IF-PSAU-2021/01/17862).

Institutional Review Board Statement: Not applicable.

Informed Consent Statement: Not applicable.

Data Availability Statement: Data are available upon request.

Conflicts of Interest: The authors declare no conflict of interest.

Nomenclature

C	Concentration	Re_x	Reynolds number
C_f	Skin friction	Sc	Schmidt number
Ec	Eckert number	Sh_x	Sherwood number
F	Dimensionless stream function	T	Temperature
f_w	Suction/blowing flow factor	(u, v)	Velocity components
g	Gravity acceleration	(x, y)	Cartesian axes
H_a	Hartmann number		Greek letters
H_0	Magnetic field intensity	μ	Effective dynamic viscosity
j	Microinertial factor	ν	Kinematic viscosity
k	Thermal conductivity	$\tilde{\xi}$	Viscosity of spin gradient
$\tilde{K}$	Dimensional porosity factor	Ω	Thermophoretic factor
K	Dimensionless porosity factor	θ	Dimensionless temperature
m	Microrotation factor	ϕ	Dimensionless concentration
N	Dimensionless angular velocity	ψ	Stream function
Nn_x	Couple stress factor	β	Micropolar coupling factor
Nu_x	Nusselt number	η	Similarity variable
Pr	Prandtl number	ϱ	Vortex viscosity
Q	Dimensionless heat source/sink factor	ρ	Active fluid density
$\tilde{Q}$	Dimensional heat source/sink factor	γ	Variable thermal conductivity factor

References

1. Agarwal, R.S.; Dhanapal, C. Flow and heat transfer in a micropolar fluid past a flat plate with suction and heat sources. *Int. J. Eng. Sci.* **1988**, *26*, 1257–1266. [CrossRef]
2. Turkyilmazoglu, M. Mixed convection flow of magnetohydrodynamicmicropolar fluid due to a porous heated/cooled de-formable plate: exact solutions. *Int. J. Heat Mass Transf.* **2017**, *106*, 127–134. [CrossRef]
3. Mahdy, A. Aspects of homogeneous-heterogeneous reactions on natural convection flow of micropolar fluid past a permeable cone. *Appl. Math. Comput.* **2019**, *352*, 59–67. [CrossRef]
4. Nazar, R.; Amin, N.; Grosan, T.; Pop, I. Free convection boundary layer on a sphere with constant surface heat flux in a micropolar fluid. *Int. Commun. Heat Mass Transf.* **2002**, *29*, 1129–1138. [CrossRef]
5. Ahmadi, G. Self-similar solution of incompressible micropolar boundary layer flow over a semi-infinite flat plate. *Int. J. Eng. Sci.* **1976**, *14*, 639–646. [CrossRef]
6. Takhar, H.S.; Agarwal, R.S.; Bhargava, B.; Jain, S. Mixed convection flow of a micropolar fluid over a stretching sheet. *Heat Mass Transf.* **1998**, *34*, 213–219. [CrossRef]
7. Ali, K.; Iqbal, M.F.; Akbar, Z.; Ashraf, M. Numerical simulation of unsteady water-based nanofluid flow and heat transfer between two orthogonally moving porous coaxial disks. *J. Theor. Appl. Mech.* **2014**, *52*, 1033–1046. [CrossRef]
8. Nabwey, H.A.; Mahdy, A. Transient flow of micropolar dusty hybrid nanofluid loaded with Fe_3O_4-Ag nanoparticles through a porous stretching sheet. *Res. Phy.* **2021**, *21*, 103777. [CrossRef]
9. Rundora, L.; Makinde, O.D. Unsteady MHD flow of non-Newtonian fluid in a channel filled with a saturated porous medium with asymmetricnavier slip and convective heating. *Appl. Math. Inform. Sci. Int. J.* **2018**, *12*, 483–493. [CrossRef]
10. Eringen, A.C. Theory of micropolar fluids. *J. Math. Mech.* **1966**, *16*, 1–18. [CrossRef]
11. Eringen, A.C. Theory of thermomicropolar fluids. *J. Math. Appl.* **1972**, *38*, 480–495.
12. Ariman, T.; Turk, M.A.; Sylvester, N.D. Microcontinuum fluid mechanics—A review. *Int. J. Eng. Sci.* **1973**, *11*, 905–930. [CrossRef]
13. Nabwey, H.A.; Mahdy, A. Numerical approach of micropolar dust-particles natural convection fluid flow due to a permeable cone with nonlinear temperature. *Alex. Eng. J.* **2021**, *60*, 1739–1749. [CrossRef]
14. Ali, K.; Ahmad, A.; Ashraf, M. Numerical simulation of flow and heat transfer in hydromagnetic micropolar fluid between two stretchable disks with viscous dissipation effects. *J. Theor. Appl. Mech.* **2016**, *54*, 633–643. [CrossRef]
15. Ali, K.; Ashraf, M. Numerical simulation of the micropolar fluid flow and heat transfer in a channel with a shrinking and a stationary wall. *J. Theor. Appl. Mech.* **2014**, *52*, 557–569.
16. Hazarika, S.; Ahmed, S. Numerical investigation of endothermic/exothermic reactionin MHD natural Convective nano-fluid flow over a vertical cone with heat source/sink. *Walailak J. Sci. Technol.* **2021**, *18*, 22834–18. [CrossRef]
17. Hazarika, S.; Ahmed, S. Brownian motion and thermophoresis behavior on micropolar nano-fluid-A numerical outlook. *Math. Comput. Simul.* **2022**, *192*, 452–463. [CrossRef]
18. Tsai, R. A simple approach for evaluating the effect of wall suction and thermophoresis on aerosol particle deposition from a laminar flow over a flat plate. *Int. Commun. Heat Mass Transf.* **1999**, *26*, 249–257. [CrossRef]
19. Talbot, L.; Cheng, R.K.; Scheffer, R.W.; Wills, D.P. Thermophoresis of particles in a heated boundary layer. *J. Fluid Mech.* **1980**, *101*, 737–758. [CrossRef]

20. Chamkha, A.J.; Camille, I. Effects of heat generation/absorption and thermophoresis on hydromagnetic flow with heat and mass transfer over a flat surface. *Int. J. Numer. Methods Heat Fluid Flow* **2012**, *10*, 432–448. [CrossRef]
21. Ahmed, S.A.; Mahdy, A. Unsteady MHD double diffusive convectionin the stagnation region of an impulsively rotating sphere in the presenceof thermal radiation effect. *J. Taiwan Institu. Chem. Eng.* **2016**, *58*, 173–180. [CrossRef]
22. Mahdy, A. Unsteady MHD slip flow of a non-Newtonian Casson fluiddue to stretching sheet with suction or blowing effect. *J. Appl. Fluid Mech.* **2016**, *9*, 785–793.
23. Waqas, M.; Farooq, M.; Khan, M.I.; Alsaedi, A.; Hayat, T.; Yasmeen, T. Magnetohydrodynamic (MHD) mixed convection flow of micropolar liquid due to nonlinear stretched sheet with convective condition. *Int. J Heat Mass Transf.* **2016**, *102*, 766–772. [CrossRef]
24. Rana, B.M.J.; Arifuzzaman, S.M.; Reza-E-Rabbi, S.; Ahmmed, S.F.; Khan, M.S. Energy and magnetic flow analysis of Williamson micropolar nanofluid through stretching sheet. *Int. J. Heat Technol.* **2019**, *37*, 487–496. [CrossRef]
25. Mahdy, A.; Ahmed, S.A. Unsteady MHD convective flow ofnon-Newtonian Casson fluid in the stagnation region of an impulsively rotating sphere. *J. Aerosp. Eng.* **2017**, *30*, 04017036. [CrossRef]
26. Sheri, S.R.; Shamshuddin, M.D. Heat and mass transfer on the MHD flow of micropolar fluid in the presence of viscous dissipation and chemical reaction. *Procedia Eng.* **2015**, *127*, 885–892. [CrossRef]
27. Shehzad, S.A.; Hayat, T.; Alsaedi, A. MHD flow of Jeffrey nanofluidwith convective boundary conditions. *J. Braz. Soc. Mech. Sci. Eng.* **2015**, *37*, 873–883. [CrossRef]
28. Rashad, A.M.; Khan, W.A.; EL-Kabeir, S.M.M.; EL-Hakiem, A.M.A. Mixed convective flow of micropolar nanofluid across a horizontal cylinder in saturated porous medium. *Appl. Sci.* **2019**, *9*, 5241. [CrossRef]
29. Arifuzzaman, S.M.; Khan, M.S.; Mehedi, M.F.U.; Rana, B.M.J.; Ahmmed, S.F. Chemically reactive and naturally convective high-speed MHD fluid flow through an oscillatory vertical porous-plate with heat and radiation absorption effect. *Eng. Sci. Technol. Int. J.* **2018**, *21*, 215–228. [CrossRef]
30. Mahdy, A.; Chamkha, A.J. Unsteady MHD boundary layer flow of tangent hyperbolic two-phase nanofluid of moving stretched porous wedge. *Int. J. Numer. Methods Heat Fluid Flow* **2018**, *28*, 2567–2580. [CrossRef]
31. Syakila, A.; Pop, I. Mixed convection boundary layer flow from a vertical flat plate embedded in a porous medium filled with nanofluids. *Int. Commun. Heat Mass Transf.* **2010**, *37*, 987–991.
32. Zehba, A.S.R.; Aly, A.M.; Ahmed, S.E. Natural convection flow of a nanofluid-filled V-shaped cavity saturated with a heterogeneous porous medium: Incompressible smoothed particle hydrodynamics analysis. *Ain Shams Eng. J.* **2021**, *12*, 2033–2046.
33. Seth, G.S.; Bhattacharyya, A.; Kumar, R.; Mishra, M.K. Modeling and numerical simulation of hydromagnetic natural convection Casson fluid flow with nth-order chemical reaction and Newtonian heating in porous medium. *J. Porous Media* **2019**, *22*, 1141–1157. [CrossRef]
34. Khedr, M.E.M.; Chamkha, A.J.; Bayomi, M. MHD flow of a micropolar fluid past a stretched permeable surface with heat gen-eration or absorption. *Nonlinear Anal. Model. Control* **2017**, *14*, 27–40. [CrossRef]
35. Hayat, T.; Ali, S.; Awais, M.; Alsaedi, A. Joule heating effects in MHD flow of Burger's fluid. *Heat Transf. Res.* **2016**, *47*, 1083–1092. [CrossRef]
36. Alreshidi, N.A.; Shah, Z.; Dawar, A.; Kumam, P.; Shutaywi, M.; Watthayu, W. Brownian motion and thermophoresis effects on MHD three dimensional nanofluid flow with slip conditions and Joule dissipation due to porous rotating disk. *Molecules* **2020**, *25*, 729. [CrossRef]
37. Hayat, T.; Qasim, M. Influence of thermal radiation and Joule heating on MHD flow of a Maxwell fluid in the presence of thermophoresis. *Int. J. Heat Mass Transf.* **2010**, *53*, 4780–4788. [CrossRef]
38. Shah, Z.; McCash, L.B.; Dawar, A.; Bonyah, E. Entropy optimization in Darcy-Frochheimer mhd flow of water based copper and silvernanofluids with Joule heating and viscous dissipation effects. *AIP Adv.* **2020**, *10*, 065137. [CrossRef]
39. Sandeep, N.; Sulochana, C. Dual solutions for unsteady mixed convective flow of MHD micropolar fluid over a stretching/shrinking sheet with non-uniformheat source/sink. *Eng. Sci. Technol. Int. J.* **2015**, *18*, 738–745.
40. Thumma, T.; Mishra, S.R. Effect of nonuniform heat source/sink, and viscous and Joule dissipation on 3D Eyring—Powell nanofluid flow over a stretching sheet. *J. Comput. Des. Eng.* **2020**, *7*, 412–426. [CrossRef]
41. Rout, B.; Mishra, S.; Thumma, T. Effect of viscous dissipation on Cu-water and Cu-kerosene nanofluids of axisymmetric radiative squeezing flow. *Heat Transf. Asian Res.* **2019**, *48*, 3039–3054. [CrossRef]
42. Naganthran, K.; Basir, M.; Thumma, T.; Olubunmi, E.; Nazar, R.; Tlili, I. Scaling group analysis of bioconvective micropolar fluid flow and heat transfer in a porous medium. *J. Therm. Anal. Calorim.* **2021**, *143*, 1943–1955. [CrossRef]
43. Thumma, T.; Magagula, V.M. Transient electromagnetohydrodynamic radiative squeezing flow between two parallel Riga plates using a spectral local linearization approach. *Heat Transf. Asian Res.* **2019**, *49*, 67–85. [CrossRef]
44. Higham, D.J.; Higham, N.J. *MATLAB Guide*; SIAM: New Delhi, India, 2005.